Atmospheric
Chemistry
and Physics
Discussions

Similarity analysis of turbulent transport and dissipation for momentum, temperature, moisture, and CO_2 during BLLAST

João A. Hackerott[1], Mostafa Bakhday Paskyabi[2], Stephan T. Kral[2], Joachim Reuder[2], Amauri P. de Oliveira[1], Edson P. Marques Filho[3], Michel d. S. Mesquita[4], and Ricardo de Camargo[1]

[1]Institute of Astronomy, Geophysics and Atmospheric Sciences, University of Sao Paulo, Sao Paulo, Brazil
[2]Geophysical Institute, University of Bergen, and Bjerknes Centre for Climate Research, Bergen, Norway
[3]Institute of Physics, Federal University of Bahia, Salvador, Brazil
[4]Uni Research Climate and Bjerknes Centre for Climate Research, Bergen, Norway

Correspondence to: J. A. Hackerott (joao.hackerott@gmail.com)

Abstract. The budget equation components for turbulent kinetic energy (TKE) and the variances of virtual potential temperature, specific humidity, and specific CO_2 content have been estimated using the Inertial Dissipation and Eddy Covariance methods. A discussion with four examples is provided about the normalization used for comparing different tracer spectra, divided by the respective characteristic scale squared. A total of 124 high frequency sample segments of a 30-min period from 20 days of the Boundary Layer Afternoon and Sunset Turbulence field campaign were used in order to provide parameterizations for the dimensionless dissipation and residual (i.e. total transport) components as a function of the Atmospheric Surface Layer (ASL) stability parameter, ζ. The results show a similar linear relation for all tracers variance dissipation components, $\Phi_\chi^D \cong 0.4 + 0.2\zeta$, during the convective ASL, i.e. $-1 < \zeta < -0.1$. Although parameterizations were also proposed for the dimensionless dissipation rate of TKE and tracer variances during stable ASL, we conclude that in this regime, other mechanisms in addition to ζ may be significantly important. In the stable and near-neutral ASL stability regimes, the transport component for different tracers may not be considered the same. In these conditions, the dissipation component of TKE and tracer variances can have the same magnitude as the other terms in their respective budget equation.

1 Introduction

The Atmospheric Surface Layer (ASL) is characterized by different turbulent flux mechanisms involving momentum and meteorological tracers (Zilitinkevich and Calanca, 2000), such as temperature, moisture and CO_2 concentration. The ASL fluxes can be estimated from their respective variance budget equations (which provide a bridge between the total variance storage and the effects

Atmospheric
Chemistry
and Physics
Discussions

of variance production, transport, and dissipation) depending on the atmospheric stability (Norman et al., 2012). Therefore, the detailed knowledge of turbulence and its fluxes is crucial in comprehensive understanding of the interactions among various processes between atmospheric physical dynamics and canopy chemical reactions (Foken et al., 2006; Ruppert et al., 2006; Sorbjan, 2009).

25   Several methodologies for quantifying the dimensionless components of the variance budget equations have been explored in the past decades, mainly for the momentum and heat (temperature and moisture) budgets (Kaimal et al., 1972; Fairall and Larsen, 1986; Edson et al., 1991; Edson and Fairall, 1998; Hartogensis and Bruin, 2005). Fewer studies, however, have considered the respective budgets of some atmospheric tracers, such as specific CO_2 content (Ohtaki, 1985; Sahlée et al.,

30   2008; Sørensen and Larsen, 2010; Sørensen et al., 2014). Nonetheless, little is known about parameterizations for the dissipation and transport components, especially for the CO_2 concentration (Iwata et al., 2005) and the stable ASL regime (Pahlow et al., 2001).

Despite the difficulty of providing expensive fast-response sensors for all different fluxes in several height levels, the most preferred technique to estimate the budget components from one level mea-

35   surements is a combination of two methods: the Eddy Covariance (EC), e.g. Aubinet et al. (2012), and the Inertial Dissipation (ID), e.g. Bluteau et al. (2011). These methods provide information about the variance dissipation and the ASL's characteristic scales by assuming the validity of the Monin-Obukhov Similarity Theory (MOST) and the Kolmogorov power law.

In this context, the height-dependent components in the normalized variance budget equations,

40   such as variance production and transport terms, need to be parameterized, usually as a function of the atmospheric stability. While the parameterizations for the mechanical and thermodynamical production terms are well-established for different budget equations (Högström, 1996; Foken, 2006; Wyngaard and Coté, 1971), little is known about the transport components due to inherent difficulties of measuring the pressure and the third-order moments of other variables. Thus, transport terms are

45   usually neglected (Fairall and Larsen, 1986; Hartogensis and Bruin, 2005; Bumke et al., 2014) or treated as a residual term in the budget equations (Yelland and Taylor, 1996; Dupuis et al., 1997; Nilsson et al., 2015).

In this study, we investigate the functional relationship between the dissipation and residual components of the variance budget equations of momentum, heat, moisture, and CO_2 concentration,

50   discussing the proposed parameterizations as a function of the ASL stability. Our analysis is based on 20 days of high frequency observations during the Boundary-Layer Late Afternoon and Sunset Turbulence (BLLAST) field experiment (Lothon et al., 2014), taken at the small-scale heterogeneity station. Considerations about how the results and the proposed methods are useful for different applications, such as studies involving air-sea interactions and canopy displacement length, are also

55   discussed.

This paper is structured as follows. In Sect. 2, we give a brief introduction on the required preprocess and quality control procedures. Section 3 formulates the budget components and the neces-

sary background about the EC and the ID methods. Section 4 evaluates and describes the results. The final section summarizes with conclusions and a brief discussion about two important applications

60   of the presented methodologies and results.

2   Description of the dataset

2.1   Measurement site and data

Measurements of wind velocity components, air temperature and the concentrations of water vapor and carbon dioxide were carried out on a $2\,\mathrm{m}$ micrometeorological mast mounted at the Surface Site

65   3 (SS3) in Site 1 from the BLLAST experiment (Lothon et al., 2014). The campaign took place in France (*Plateau de Lannemezan*), a few kilometers North of the foothills of the Pyrenees, from 14th June to 8th July, 2011. The area around SS3 is characterized by a flat surface ($150 \times 150\,\mathrm{m}^2$) covered mainly by short grass. The measuring system for sampling frequency of 20 Hz includes a sonic anemometer CSAT3 for collecting data of temperature and wind velocity, a gas analyzer LICOR

70   7500 for monitoring the concentrations of H_2O and CO_2, and a Paroscientific microbarometer for measuring the air pressure, as illustrated in Fig. 1.
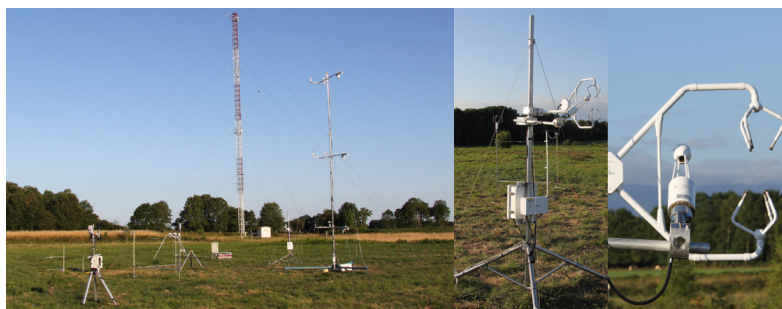

Figure 1. Field setup (left) of Surface Site 3 in Site 1 of the BLLAST campaign, micrometeorological mast (middle), and detail of the sonic anemometer CSAT3 and the gas analyzer LICOR 7500 (right).

The temperature was converted to the virtual potential temperature using the moisture and pressure data. From now on, the temperature or the potential temperature (θ) will be referred to as virtual potential temperature. Considering the pressure and the air temperature, and neglecting the moisture

75   effect on the air density, the H_2O and CO_2 concentrations were converted to the specific humidity (q) and specific CO_2 content (c), in $[\mathrm{mg\,kg}^{-1}]$. Additionally, the wind data was rotated into the streamwise wind (i.e. $\overline{v} = \overline{w} = 0$), following Lee et al. (2005), for every 15-min segment, which is the interval length applied for the ID method.

Atmospheric
Chemistry
and Physics

Open Access

EGU

Discussions

2.2 Quality assessment of the dataset

80 Based on solar radiation data (Lothon et al., 2014), 20 days with low cloud coverage have been selected for this study. Thus, the 14th, 15th, 24th and 30th days of June from the BLLAST campaign have not been considered.

In order to reduce the effect of flow distortion induced by the probes and the mast, the dataset was limited to the undistorted sector by removing the wind data that comes from a sector of $\pm 30°$ in the

85 foremast direction (Li et al., 2013).

The data also underwent a conventional spike removal algorithm (Foken et al., 2005). It is considered for this study only 30-min segments with more than 95% of the original length preserved.

The EC and ID methods are based on the assumption of stationarity. The steady state test was applied for the three wind velocity components by dividing every 30-min segment into four equal

90 intervals and comparing the variances among them. If the variances deviate more than 50% compared to the lowest variance within the segment, the whole segment is discarded.

The so-called Ogive test for $\overline{u'w'}$ (Foken et al., 2006) was applied as an additional quality test, where u' and w' are the horizontal and vertical velocity fluctuation components. This test is used to describe the distribution of the covariances across the frequency domain, verifying if the segment

95 encloses all the turbulent eddies that contribute to the overall flux. The ogive curves, $Og_{u'w'}$, are defined by taking the cumulative integral of the turbulent flux co-spectrum ($Co_{u'w'}$), starting with the highest frequency:

$$Og_{u'w'}(n) = \int_{\infty}^{n} Co_{u'w'}(n)dn. \tag{1}$$

100 The test compares the $Og_{u'w'}$ for two distinct frequencies, n, and evaluates the rate R_{Og}, defined in Eq. (2). In this study, the 0.5-hour (0.5h) segments were expanded one hour back and one hour forward, in order to have a larger segment of 1.5-hour (1.5h). If R_{Og} was greater than the threshold 90%, it was assumed that the ogive converged and the original segment is large enough to satisfy that low frequency parts are included in the measured turbulent flux. Here, 81% of the total available

105 segments were accepted after this test.

$$R_{Og} = \left| \frac{Og(n_{0.5h})}{max[Og(n_{1.5h})]} \right|. \tag{2}$$

The validity of the Taylor Hypothesis was examined considering only segments where the standard deviation of the streamwise wind, in isotropic turbulent flows, was smaller than half of the mean wind

110 velocity (Willis and Deardorff, 1976).

Atmospheric
Chemistry
and Physics
Discussions

A few segments were rejected after visual inspection of all automatically qualified datasets. A total of 124 segments of 30-min period are labeled as accepted and used in the present analysis. The data contains most of the whole 24-hour day period, with gaps on the hours 11.25, 15.25, 18.25 and 19.25 UTC, when no segment was accepted. The averages and standard deviations of the observed

115 wind magnitude, θ, q, and c are $2.1 \pm 0.9\,\mathrm{m\,s^{-1}}$, $295 \pm 5\,\mathrm{K}$, $14 \pm 3\,\mathrm{g\,kg^{-1}}$, and $746 \pm 39\,\mathrm{mg\,kg^{-1}}$, respectively.

3 Budget of the scalar variances

3.1 The budget equations of the variances

The variance budget equations for the momentum (commonly referred to as Turbulent Kinetic En-

120 ergy, TKE) and the different scalars χ_i (i.e. $\chi_1 = \theta$; $\chi_2 = q$; $\chi_3 = c$), for the isotropic homogeneous turbulent flow, in the absence of subsidence, can be expressed as follows:

$$\frac{1}{2}\frac{\partial \overline{u'^2}}{\partial t} = -\overline{u'w'}\frac{\partial \overline{u}}{\partial z} + \frac{g}{\theta_0}\overline{\theta'w'} - \frac{\partial \overline{u'^2 w'}}{\partial z} - \frac{1}{\rho_0}\frac{\partial \overline{p'w'}}{\partial z} - \epsilon, \tag{3}$$

$$\frac{1}{2}\frac{\partial \overline{\chi_i'^2}}{\partial t} = -\overline{\chi_i'w'}\frac{\partial \overline{\chi_i}}{\partial z} - \frac{1}{2}\frac{\partial \overline{\chi_i'^2 w'}}{\partial z} - N_{\chi_i}, \tag{4}$$

125 where ϵ is the dissipation rate of TKE, N_{χ_i} the dissipation rates of the tracer variances, g the gravitational acceleration, θ_0 the reference virtual potential temperature, ρ_0 the reference air density, z the height above surface, and p' the atmospheric pressure fluctuation. Overbars and primes are used to denote Reynolds averages and fluctuations from this average, respectively. It is worth mentioning that the effect of roughness length on the observational height z is neglected, since deviations of the

130 order of a few centimeters in z would induce much smaller uncertainties than other factors involved in the EC and ID methods.

For homogeneous turbulence within the ASL, the MOST asserts that the vertical turbulent fluxes are described by characteristic scales. Rewriting Eqs. (3) and (4) in a dimensionless form, and assuming stationary conditions, gives:

135
$$\underbrace{\frac{\kappa z}{u_*}\frac{\partial \overline{u}}{\partial z}}_{\Phi^M} - \underbrace{\frac{\kappa z \theta_*}{u_*{}^2}\frac{g}{\theta_0}}_{\zeta} - \underbrace{\left[\frac{\kappa z}{u_*{}^3}\frac{\partial \overline{u'^2 w'}}{\partial z} + \frac{\kappa z}{u_*{}^3}\frac{1}{\rho_0}\frac{\partial \overline{p'w'}}{\partial z}\right]}_{\Phi_u^T} - \underbrace{\frac{\kappa z}{u_*{}^3}\epsilon}_{\Phi_u^D} = 0, \tag{5}$$

$$\underbrace{\frac{\kappa z}{\chi_{i_*}}\frac{\partial \overline{\chi_i}}{\partial z}}_{\Phi_{\chi_i}^H} - \underbrace{\frac{\kappa z}{2 u_* \chi_{i_*}{}^2}\frac{\partial \overline{\chi_i'^2 w'}}{\partial z}}_{\Phi_{\chi_i}^T} - \underbrace{\frac{\kappa z}{u_* \chi_{i_*}{}^2}N_{\chi_i}}_{\Phi_{\chi_i}^D} = 0, \tag{6}$$

Atmospheric
Chemistry
and Physics
Discussions

where κ is the von Kármán constant ($\kappa \approx 0.4$), Φ^M the dimensionless mechanical production of TKE, and $\Phi_{\chi_i}^H$ the dimensionless thermodynamic production of χ_i variance. The superscript T indicates the transport and D the dissipation dimensionless components, and the subscript $*$ is a reference to the ASL characteristic scale. The buoyancy component (ζ) is, by definition, the Monin-Obukhov stability parameter, with negative values indicating convective and positive values indicating stable conditions within the ASL. Furthermore, according to MOST, Φ^M and $\Phi_{\chi_i}^H$ are universal functions, which depend only on ζ. Finally, the vertical transport of TKE and the divergence of pressure transport in Eq. (5) are treated as the total transport of TKE, Φ_u^T.

There are several parameterizations available in the literature for Φ^M and $\Phi_{\chi_i}^H$. According to the review of Foken (2006), the most acceptable universal functions for momentum, sensible heat and water vapor are described by Högström (1996), valid for $-2 < \zeta < 0.5$. Therefore, we parameterize the mechanical and thermodynamical production terms as follows:

$$\Phi^M = \begin{cases} (1-19\zeta)^{-\frac{1}{4}}, & \zeta \leq 0 \\ 1+5.3\zeta, & \zeta > 0 \end{cases} \tag{7}$$

$$\Phi^H = \begin{cases} (0.95(1-11.6\zeta)^{-\frac{1}{2}}, & \zeta \leq 0 \\ 1+8\zeta, & \zeta > 0 \end{cases} \tag{8}$$

Considering that Eq. (8) is invariant to the tracer type (i.e. $\Phi^H = \Phi_{\chi_i}^H$), also suggested by other authors, e.g. Dyer (1974); Hill (1989), an equation for the dissipation rates of different tracer variances can be expressed as:

$$\frac{N_{\chi_i}}{\chi_{i*}^2} = \frac{u_*}{\kappa z} \left(\Phi^H - \Phi_{\chi_i}^T \right). \tag{9}$$

Considering the spectral theory (explained in Sect. 3.3), Eq. (9) suggests that the usual spectra normalization (Sahlée et al., 2008), power spectra divided by the squared characteristic scale, originally proposed by Kaimal et al. (1972), makes the spectra collapse within the inertial subrange only if the transport term is also invariant to the tracer type. Analogously, this fact can be also observed for the TKE power spectrum in neutral conditions ($\zeta = 0$), when $\Phi^M \approx \Phi^H$.

The dissipation components are usually parameterized as functions of ζ, as summarized by Hill (1997). It is consensus to distinguish the parameterization for different stability regimes, however, the proposed functions vary considerably in their general shape, the corresponding coefficients, and the stability range they are defined for (e.g. Wyngaard and Coté, 1971; Ohtaki, 1985; Kader, 1992; Hartogensis and Bruin, 2005; Pahlow et al., 2001). Based on the present results, it is assumed linear function for $\Phi^D(\zeta)$ in the different stability regimes. In the special case of near-neutral conditions, Φ^D is balanced by $[1 - \Phi^T]$, which might not be a constant like the mechanical production component. Beyond that, from Eq. (6), one can follow $\lim_{\zeta \to 0} \Phi_\theta^D = \infty$, as it was observed by Kader (1992), which will be discussed in Sect. 3.2. Thus, the dissipation component analysis is limited to $|\zeta| > 0.1$.

Atmospheric
Chemistry
and Physics
Discussions

Since Φ^T is regarded as a residual term in Eqs. (5) and (6), its parameterization is then defined in this study as:

$$\Phi_u^T = \Phi^M - \Phi_u^D - \zeta\,, \quad |\zeta| > 0.1 \tag{10}$$

175

$$\Phi_{\chi_i}^T = \Phi^H - \Phi_{\chi_i}^D\,, \quad |\zeta| > 0.1 \tag{11}$$

3.2 The ASL characteristic scale

The EC method computes the second-order moments directly from a high-frequency dataset. Ac-
180 cording to MOST, the ASL characteristic scale for wind velocity (i.e. friction velocity) and tracers are defined in terms of these second-order moments as follows:

$$u_* = \left[\left(\overline{u'w'}\right)^2 + \left(\overline{v'w'}\right)^2\right]^{\frac{1}{4}}, \tag{12}$$

$$\chi_{i_*} = -\frac{\overline{\chi_i'w'}}{u_*}. \tag{13}$$

185

Regardless of the simplicity of these equations, special care must be taken in order to guarantee two main hypotheses, i.e. the stationarity of the flow, and the representation of all relevant scales of turbulent eddies in their respective covariances. While the first suggests short period segments, the second suggests longer period segments. In order to meet both criteria in the best possible way,
190 we decided to use 30-min segments to estimate the characteristic scale values. The aforementioned quality control and assurance procedure satisfied both hypotheses reasonably.

It is noteworthy that, in the absence of a tracer flux, the characteristic scale values in Eq. (13) vanish (i.e. $\chi_{i_*} = 0$), and then all terms in Eq. (6) become undefined. Nevertheless, observations indicate that, in neutral conditions, Φ^M and Φ^H asymptotically approach a constant (Dyer, 1974;
195 Högström, 1996). Also, $\theta_* \to 0$ only when $\zeta \to 0$, and then the singularity occurs just during neutral ASL for the equations involving temperature. However, this is not the case for q_* and c_*, for which the sign is asserted by the corresponding vertical gradient direction, that is not necessarily correlated to ζ. Then, in order to evaluate the behavior of universal functions against ζ, the segments with $|q|_* < 0.01\,\mathrm{g\,kg^{-1}}$ and $|c|_* < 0.1\,\mathrm{mg\,kg^{-1}}$ were excluded. The Taylor Hypothesis test performed in
200 the quality control is sufficient to guarantee $u_* \not\approx 0$, avoiding singularities in Eqs. (13), (5) and (6).

3.3 Spectral theory

According to the Kolmogorov power law, there is a range of wave numbers, k, within the momentum energy spectrum, S_u, called inertial subrange, where the energy is transferred from large scale eddies

Atmospheric
Chemistry
and Physics
Discussions

to small scale ones, at a constant dissipation rate of TKE, ϵ. Within this inertial subrange the energy

205 production and dissipation, are sufficiently smaller than the spectral density of the streamwise wind velocity, which then depends only on k and ϵ. This theory, originally formulated by Kolmogorov (1941) for the momentum variance spectrum, was later implemented for heat (Corrsin, 1951), moisture (Edson et al., 1991), and specific CO_2 content (Sørensen and Larsen, 2010; Sahlée et al., 2008).

Considering the Taylor Hypothesis of "frozen" turbulence, it is possible to express S in terms

210 of frequency, n, instead of k. Therefore, within the inertial subrange, the spectral densities may be expressed in terms of frequency power spectrum of longitudinal wind velocity, $S_u(n)$, and tracers, $S_{\chi_i}(n)$:

$$S_u(n) = \alpha \epsilon^{\frac{2}{3}} n^{-\frac{5}{3}} \left(\frac{2\pi}{U} \right)^{-\frac{2}{3}}, \tag{14}$$

215 $$S_{\chi_i}(n) = \beta \epsilon^{-\frac{1}{3}} n^{-\frac{5}{3}} N_{\chi_i} \left(\frac{2\pi}{U} \right)^{-\frac{2}{3}}, \tag{15}$$

where U is the mean longitudinal wind velocity, $\alpha = 0.52$ is the Kolmogorov constant, and $\beta = 0.8$ is the Obukhov-Corrsin constant, following Högström (1996). It is assumed in this study that β is invariant to the tracers type (Hill, 1989; Iwata et al., 2005). As a consequence of isotropy, Eq. (14) can also be expressed for the vertical and transversal wind components, w and v, using $\alpha_v = \alpha_w = \frac{4}{3}\alpha_u$

220 (Kaimal et al., 1972).

The spectral densities are computed using the Fast Fourier Transform (FFT). This technique, however, requires additional data treatment in order to reduce undesirable inherent noise (Stull, 1988). Thus, the segments were detrended and 5% tapered by the Tuckey Window function (Bloomfield, 2000).

225 The segment length is crucial for the ID method. Based on visual inspection of the spectral signals, we decided to use segments of 18,000 data samples (15-min), which is large enough to ensure that the low-frequency limit of the inertial subrange is well resolved in the FFT result. The ID method is very sensitive to the stationarity assumption (Bluteau et al., 2011), which is more likely to be violated when using longer data segments (e.g. 30-min segment) and thus causing elevated values

230 of the spectral density due to the white noise.

After providing $S_u(n)$, ϵ is estimated from Eq. (14) using a nonlinear fit within the inertial subrange. N_{χ_i} is then estimated, also by applying a nonlinear fit, based on Eq. (15), to the respective inertial subrange of $S_{\chi_i}(n)$. The inertial subrange interval is estimated using the inertial subrange detector method, described in Appendix A.

235 In order to combine the results from the EC and ID methods, which are estimated for different segment lengths, it is necessary to convert the dissipation rates calculated for the 15-min segment to the 30-min segment. For this, we propose an iterative methodology. First, the 30-min intervals are enlarged 14-min back and forward, resulting in 69,600 data samples. Within the iterative process,

Atmospheric
Chemistry
and Physics
Discussions

the dissipation rates for a 15-min interval are calculated, starting at the beginning of the extended
segment. This procedure is then repeated by moving the start point with a time step of 1-min until
the end of the extended segment is reached. This iteration ensures that almost all data of the original
30-min interval (excluding the first and last 1 min period) are weighted equally. The dissipation rate
for the 30-min segment is then defined as the median of the 44 iterations. We use median instead
of the mean to prevent the influence of eventual overestimated dissipation rates originated from
non-stationarities.

4   Results

Following the premise that the variance budget components may be expressed as a function of ζ, the
results in this section are classified into three ASL stability regimes, convective ($\zeta < -0.05$), near-
neutral ($|\zeta| \leq 0.05$), and stable ($\zeta > 0.05$), distinguished by three different colours in the presented
figures.

Our results will be discussed in three parts: first a discussion of MOST parameters and dissipation
rates derived by the EC and ID methods; second the examination of the dissipation and residual
components of the variance budget equation; and finally a discussion of four selected examples.

4.1   MOST parameters and dissipation rates

The time series of the Monin-Obukhov stability parameter and the ASL characteristic scale values
are displayed in Fig. 2, where the colours distinguish the stability regimes, blue for the stable, red
for the convective, and black for the near-neutral. The 124 available segments covered in a similar
quantity all the three regimes, 35% for the convective, 27% for the stable, and 38% the near-neutral
regime. The ζ ranges from -0.99 to 1.06, with five occurrences with $\zeta \geq 0.5$, which are out of the
validity range of Eqs. (7) and (8).

The friction velocity, u_*, significantly oscillates depending on the ASL stability regime. It is
observed $u_* = 0.22 \pm 0.07 \, \mathrm{m \, s^{-1}}$ for the segments collected during the convective ASL, while for
the stable regime, $u_* = 0.12 \pm 0.04 \, \mathrm{m \, s^{-1}}$, excluding the observations done during the night time
between June 26th and 27th. The segments measured during this night registered an elevated mean
wind velocity, $3.4 \pm 0.2 \, \mathrm{m \, s^{-1}}$, and consequently high values for u_*, $0.280 \pm 0.016 \, \mathrm{m \, s^{-1}}$. In general,
during the convective ASL regimes, the wind velocity was also higher ($2.1 \pm 0.9 \, \mathrm{m \, s^{-1}}$) than during
the stable ASL, when it was registered a mean wind velocity of $1.4 \pm 0.6 \, \mathrm{m \, s^{-1}}$, excluding the
referred night.

The stability regimes are visually correlated to the characteristic scale values, θ_*, q_*, and c_*. From
the definition of ζ, it is assigned to the same sign as θ_*, however, for q_* and c_*, the flux direction
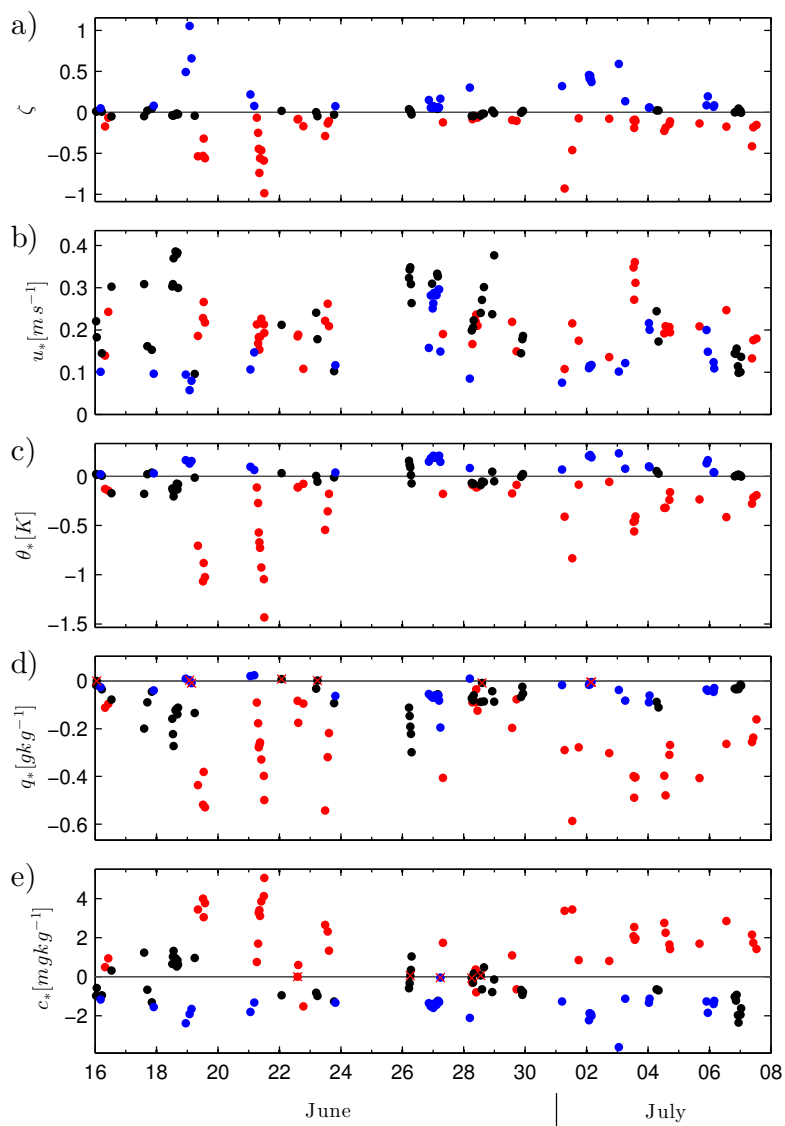is less dependent on the stability. During the night time (most likely stable regime), due to the

Atmospheric
Chemistry
and Physics
Discussions

Open Access

EGU

Figure 2. Times series, estimated for 30-min segments collected during the 2011 BLLAST campaign, of: (a) Monin-Obukhov stability parameter (ζ); (b) friction velocity [$\mathrm{m\,s^{-1}}$]; (c) characteristic scales of virtual potential temperature [K]; (d) characteristic scales of specific humidity [$\mathrm{g\,kg^{-1}}$]; and (e) characteristic scales of specific CO_2 content [$\mathrm{g\,kg^{-1}}$]. The colours indicate the ASL stability regimes, convective (red), near-neutral (black), and stable (blue). The red crosses on (d) and (e) indicate the data that are not considered for the calculation of the dissipation and residual components of variance budget equations.

Atmospheric
Chemistry
and Physics
Discussions

lower temperature, the relative humidity is higher, and consequently the vertical moisture gradient is weaker, considering a near saturated soil. In this condition, however, the ASL is still dryer than the ground below, which provides an upward moisture flux ($q_* < 0$) also for the stable regimes.

The time series of c_* is also correlated to ζ and $\theta_* > 0$, however, as observed for q_*, the sign of c_* does not necessarily follow the sign of ζ, as it is observed on the days 22nd, 28th, and 29th of June. The sign of c_* follows the photosynthesis activity, being positive usually during the daytime. The magnitude of all ASL characteristic scale values are affected by the ASL turbulence, increasing when the turbulent eddies are stronger, either because of mechanical or buoyant turbulence production.

The seven segments of q_* and five segments of c_*, marked with a red cross in Fig. 2 are rejected from the analysis of variance budget components, since they result on singularities in Eq. (6), regardless of the ASL stability regime.

The ID method is used in the calculation of the dissipation rates. The spectra of all segments were visually analyzed for the three wind components and we decided for using the vertical velocity in Eq. (14), due to the more stationary state of this component when compared to the horizontal ones. This observation was also commented by Nilsson et al. (2015) in their study for the afternoon transition of TKE budget, using the BLLAST dataset, but from a different micrometeorological tower.

Figure 3 summarizes the dissipation rates for the BLLAST datasets that could be estimated. Similar to what is observed for u_*, the dissipation rate of TKE is more sensitive to the wind magnitude. We highlight the afternoon of June 18th and the morning of June 26th, when although the stability is labeled as near-neutral, it was registered relatively strong winds and, consequently, higher values of u_* and ϵ are observed.

Despite the fact that the dissipation rates of θ, q, and c variances are related to ϵ, in Eq. (15), the magnitude of the dissipation rates of these tracers are more sensitive to their respective fluxes than the wind variation. This fact is well observed on the segments collected during June 21st, July 1st and 3rd, when the intensity of the dissipation rates follow almost the same pattern observed for the characteristic scale values. Thus, the N_θ, N_q, and N_c are also correlated with ζ, mainly for the convective period (day time) as it was explained before for the ASL characteristic scales.

4.2 Dissipation and residual components in the variance budget equation

The dimensionless dissipation rates, Φ^D, are presented in Fig. 4 with respect to the different stability regimes, convective (red), near-neutral (black), and stable (blue). Using the BLLAST data, we fit the dissipation rates by the following $\zeta-$dependent linear relationship:

$$\Phi^D = \zeta \, a^\pm + b^\pm, \tag{16}$$

where the superscripts indicate convective ($-$) and stable ($+$) regimes, and $a^\pm$ and $b^\pm$ are the slope and intercept coefficients for the linear regression, respectively.
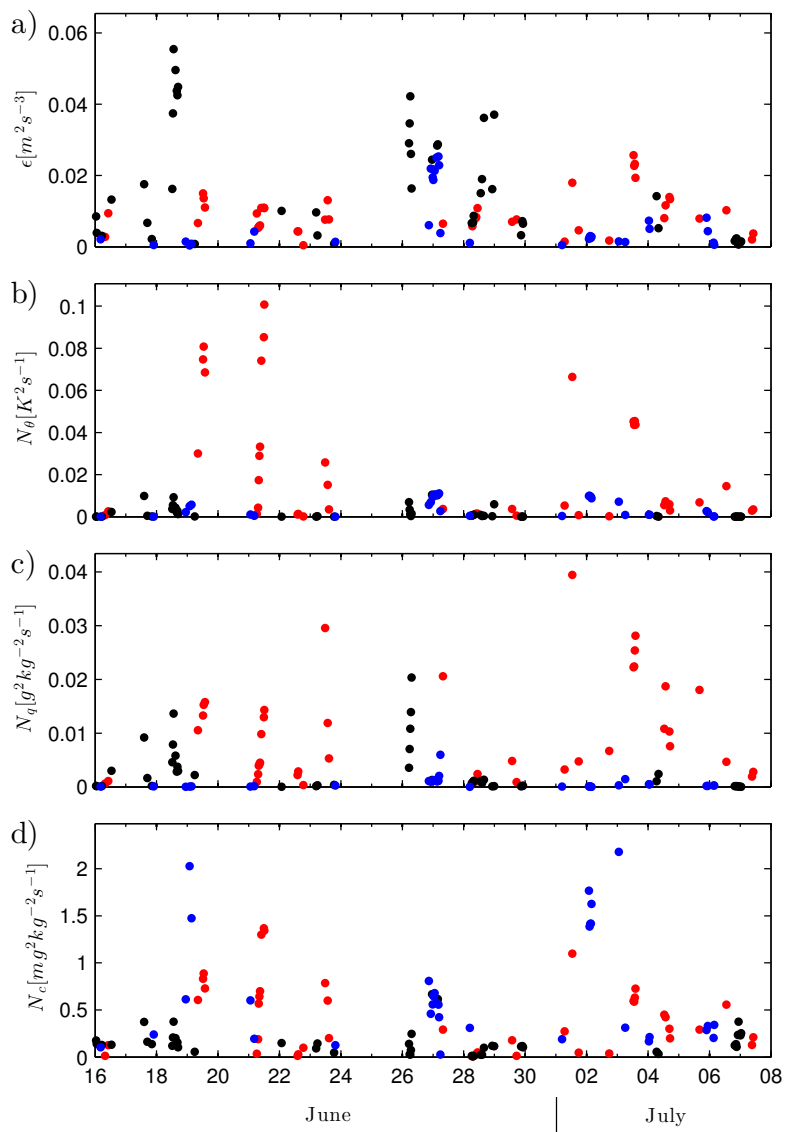
Atmospheric
Chemistry
and Physics
Discussions

Figure 3. Times series, estimated for 30-min segments collected during the 2011 BLLAST campaign, of the dissipation rates of: (a) TKE $[\mathrm{m^2\,s^{-3}}]$; (b) the virtual potential temperature variance $[\mathrm{K^2\,s^{-1}}]$; (c) the specific humidity variance $[\mathrm{g^2\,kg^{-2}\,s^{-1}}]$; and (d) the specific CO_2 content variance $[\mathrm{g^2\,kg^{-2}\,s^{-1}}]$. The colours indicate the ASL stability regimes, convective (red), near-neutral (black), and stable (blue).
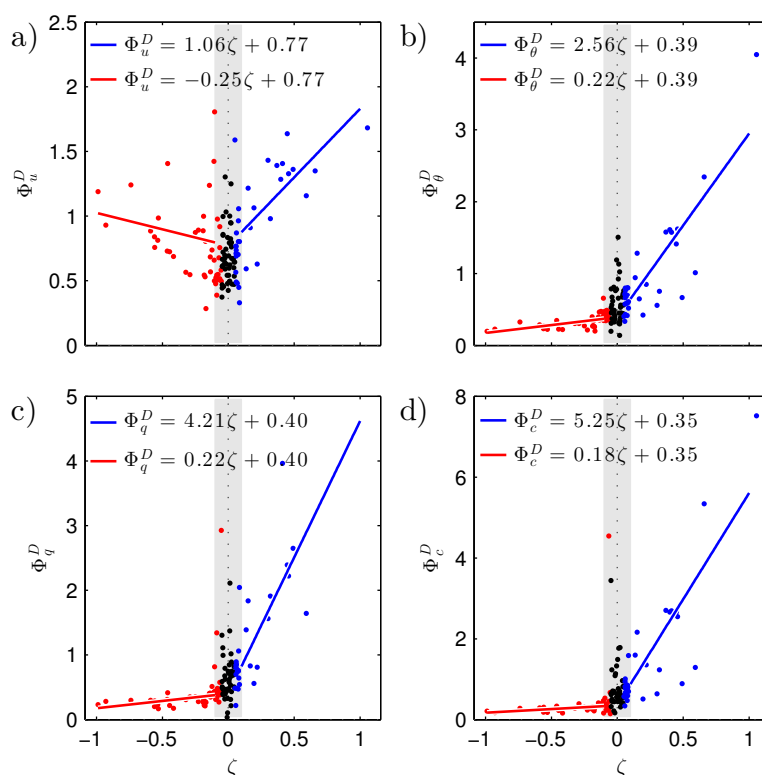
Figure 4. Scatterplot of the dimensionless dissipation component (Φ^D) against the Monin-Obukhov stability parameter (ζ) for the budget equation of: (a) TKE; (b) variance of virtual potential temperature (θ); (c) variance of specific humidity (q); and (d) variance of specific CO_2 content (c). The colours indicate the ASL stability regimes, convective (red), near-neutral (black), and stable (blue). The red and blue lines are the linear regressions estimated for the convective and stable regime, respectively. The gray area corresponds to $|\zeta| \leq 0.1$, where the data is not considered for the linear fit.

Atmospheric
Chemistry
and Physics

Discussions

Open Access

The scatterplots of the Φ^D against ζ show that it is difficult to find an appropriate functional

310   form for the stable regimes due to the high scattering (i.e. relatively high Root Mean Square Error, $RMSE$) and the small values for the correlation coefficients of the fitting curves (i.e. $R^2 < 0.7$). Thus, we held the same intercept coefficient for the stable regime as the one estimated for the convective regime, resulting in a decreased degree of freedom for the linear regression on the stable ASL datasets. Furthermore, it is evident on the results for Φ_q^D and Φ_c^D that the range defined for

315   near-neutral conditions ($|\zeta| \leq 0.05$) is not enough to avoid the effect of singularities, described on Sect. 3.1 and 3.2. Therefore, we decided to enlarged this range for $|\zeta| \leq 0.1$ (gray shaded area in Fig. 4) in order to provide a less biased parameterization. The slope and intercept coefficients are summarized in Table 1, together with their respective R^2 and $RMSE$.

Table 1. Coefficients $a^{\pm}$ and $b^{\pm}$ for regression defined in Eq. (16). R^2 and $RMSE$ are the squared correlation coefficient and the root mean square error, respectively.

		Φ_u^D	Φ_θ^D	Φ_q^D	Φ_c^D
Convective	b^-	0.77	0.39	0.40	0.356
	a^-	-0.25	0.22	0.22	0.18
	R^2	0.04	0.28	0.19	0.28
	$RMSE$	0.31	0.09	0.11	0.07
Stable	b^+	0.77	0.39	0.40	0.356
	a^+	1.06	2.56	4.21	5.26
	R^2	0.42	0.66	0.32	0.62
	$RMSE$	0.23	0.50	0.74	1.1

320   Although R^2 is lower for the convective ASL regimes, the $RMSE$ is much lower in this regime compared to the stable ASL, indicating more precision of the regression curves during the convective regime. The results for Φ_u^D show a weak relation with ζ for both the convective and the stable regimes. As mentioned in Sect. 4.1, the dissipation rate of TKE is sensitive to the wind velocity, which therefore is more affected by the mesoscale atmospheric conditions than the local turbulence

325   characteristics. While there are several possible factors that influence the quality of the Φ_u^D measurements, we conclude that its parameterization should include the effect of mean wind velocity as also recommended by Yelland and Taylor (1996). They proposed to divide the observed data into three wind regimes: $3 - 7$, $10 - 12$ and $17 - 20 \, \mathrm{m \, s^{-1}}$, respectively. However, the BLLAST datasets fall only within the first recommended range, which emphasizes the need for considering more relevant

330   mechanisms rather than only ζ.

The high scattering on stable ASL regime has also been reported by other studies (e.g., Pahlow et al., 2001; Hartogensis and Bruin, 2005; Nilsson et al., 2015), and as a consequence, the available parameterizations vary substantially in the literature. For example, Pahlow et al. (2001) found $a^+ = 5$ and $b^+ = 0.61$, while Hartogensis and Bruin (2005) found $a^+ = 2.5$ and $b^+ = 8$ for Φ_u^D. The only

335 consensus is that Φ_u^D increases as the ASL becomes more and more stable. For Φ_χ^D, however, there is no consensus in the literature and few parameterizations are available. Pahlow et al. (2001) suggests a constant value near to unity in the range $0 < \zeta < 100$, although their data varies randomly between 0.1 and 10. In general, the data presented in Fig. 4 shows an increasing magnitude of Φ^D on stable ASL and significant differences between the slope coefficients of the parameterizations for different

340 tracers.

The parameterizations for $\Phi_{\chi_i}^D$, within the convective regimes, are approximately identical, i.e. $a^- \cong 0.2$ and $b^- \cong 0.4$. These values are in agreement with the results from Ohtaki (1985) for c, and Kader (1992) for θ and q. Although they proposed different function shapes, their curves can be approximated by linear functions in the stability range, $-1 < \zeta \leq -0.2$, with a similar slope and

345 slightly higher magnitudes than those observed from this study. For $-0.2 < \zeta < -0.1$, the parameterizations proposed by Kader (1992) and Ohtaki (1985) cannot be considered linear and increase rapidly in magnitude. This fact may be a consequence of the influence of the singularities that occur in near-neutral regimes for the tracers and were not neglected by these authors. Note that the formulations proposed by Kader (1992) need to be multiplied by the von Kármán constant in order to

350 compare to our results.

The transport components, Φ^T, are estimated as a residual term in the variance budget equations. The analysis is restricted to the stable range for $\zeta < 0.5$ because the parameterization for Φ^M and Φ^H, Eqs. (7) and (8), are specified for this range. Thus, the proposed parameterization curves, derived from Eqs. (10) and (11), are expressed according to Eqs. (17) and (18), with coefficients $a^\pm$

355 and $b^\pm$ summarized in Table 2.

$$\Phi_u^T = \begin{cases} (1 - 19\zeta)^{-\frac{1}{4}} + \zeta\,a^- + b^-\,, & -1 < \zeta < -0.1 \\ b^+ + \zeta\,a^+\,, & 0.1 < \zeta < 0.5 \end{cases} \tag{17}$$

$$\Phi_{\chi_i}^T = \begin{cases} 0.95(1 - 11.6\zeta)^{-\frac{1}{2}} + \zeta\,a^- + b^-\,, & -1 < \zeta < -0.1 \\ b^+ + \zeta\,a^+\,, & 0.1 < \zeta < 0.5 \end{cases} \tag{18}$$

360 The scatterplots for $\Phi_{\chi_i}^T$ against ζ, presented in Fig. 5, indicate the convergence to low values in the convective regimes, showing that these terms can be neglected. On the other hand, it is clear that the importance of the Φ^T, on the stable regime increases as the ASL becomes more stable, when

Atmospheric
Chemistry
and Physics
Discussions

Table 2. Coefficients $a^\pm$ and $b^\pm$ for the regressions defined in Eqs. (17) and (18).

		Φ_u^T	Φ_θ^T	Φ_q^T	Φ_c^T
Convective	b^-	-0.77	-0.39	-0.40	-0.36
	a^-	-0.75	-0.22	-0.22	-0.18
Stable	b^+	0.23	0.61	0.60	0.65
	a^+	3.24	5.44	3.79	2.74

the estimated magnitudes of Φ^T are comparable to the other components of the respective budget equation, also for Φ_u^T.

365　Although high scatter is observed for Φ_u^T, the proposed parameterization for $-1 < \zeta < -0.1$ is in agreement with the results from other studies, such as Dupuis et al. (1997), who proposed a linear curve $\Phi_u^T = -0.65\zeta$ for $-7 < \zeta < 0$, and Nilsson et al. (2015) which the parameterization is approximated for $\Phi_u^T = -0.5\zeta$ when $-8 < \zeta < 0$. The curves proposed by these authors suggest a
370　convergence to low values in near-neutral stability regimes, in agreement with Fairall and Larsen (1986) who suggested that Φ_u^T is about 25% of Φ_u^D in this regime. Our results, however, show that the mean ratio between Φ_u^T and Φ_u^D for $|\zeta| \leq 0.05$ is 0.6 ± 0.4.

4.3 Case examples

In this section, four 30-min segments are selected with the following ASL stability characteristics
375　for a detailed analysis:

1. June 21st, $11:45:00$ UTC - Convective ($\zeta = -0.6$);

2. June 27th, $00:15:00$ UTC - Low stable ($\zeta = 0.08$);

3. June 18th, $13:15:00$ UTC - Near-neutral ($\zeta = -0.04$);

4. June 18th, $22:45:00$ UTC - Stable ($\zeta = 0.5$).

380　The estimated components of the variance budget equations, Eqs. (5) and (6), are summarized in Table 3 together with the respective dissipation rates normalized by the squared characteristic scale.

Although Cases 2 and 3 are in a stability regime away from the validity of the proposed functions (i.e. $|\zeta| \leq 0.1$), the parameterizations for the dissipation rate enclose all cases with exception of Case
385　4 for Φ_θ^D and Φ_c^D, considering an acceptable error of 20%. In Case 4, which is an example of the ASL stable regime, the estimated Φ_θ^D and Φ_c^D are 2.5 and 3.3 times greater than the values expected from the suggested parameterizations.

16

Atmospheric
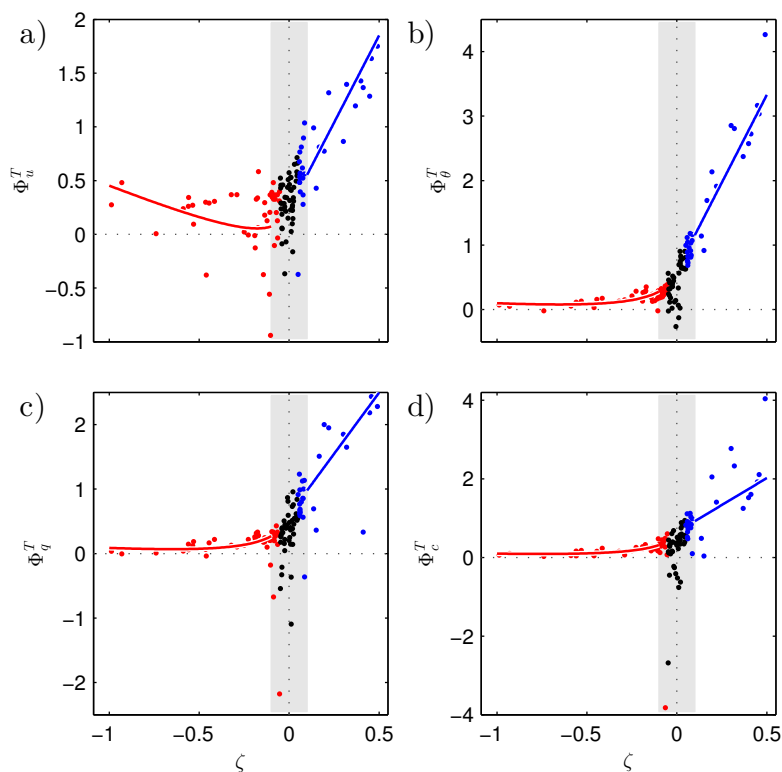Chemistry
and Physics
Discussions

Figure 5. Scatterplot of the dimensionless total transport component (Φ^T) against the Monin-Obukhov stability parameter (ζ) for the budget equation of (a) TKE; (b) variance of virtual potential temperature (θ); (c) variance of specific humidity (q); and (d) variance of specific CO_2 content (c). The colours indicate the ASL stability regimes convective (red), near-neutral (black), and stable (blue). The lines are the total transport components estimated as a residual of the variance budget equations, considering the suggested parameterizations for the dimensionless dissipation and dynamical production components. The gray area corresponds to $|\zeta| \leq 0.1$, where the data is not considered for the parameterizations.

Atmospheric
Chemistry
and Physics
Discussions

Table 3. Monin-Obukhov stability parameter (ζ), mechanical (Φ^M) and thermodynamical (Φ^H) production, dissipation (Φ^D), and transport (Φ^T) components of the variance budget equations, and the ratio between the dissipation rates and the corresponding squared characteristic scale in unit of [s^{-1}], for TKE, virtual potential temperature (θ), specific humidity (q), and specific CO_2 content (c), for the four Cases.

Case:	1	2	3	4
ζ	-0.6	0.08	-0.04	0.5
Φ^M	0.5	1.4	0.9	3.6
Φ^H	0.3	1.6	0.8	4.9
Φ_u^D	0.9	0.8	0.9	1.4
Φ_θ^D	0.3	0.7	0.5	0.7
Φ_q^D	0.3	0.8	0.4	2.7
Φ_c^D	0.3	0.8	0.5	0.9
Φ_u^T	0.24	0.52	0.05	1.75
Φ_θ^T	0.05	0.91	0.32	4.26
Φ_q^T	0.04	0.86	0.40	2.28
Φ_c^T	0.05	0.85	0.33	4.04
$\frac{\epsilon}{u_*^2}$	0.24	0.27	0.41	0.16
$\frac{N_\theta}{\theta_*^2}$	0.08	0.24	0.22	0.08
$\frac{N_q}{q_*^2}$	0.08	0.25	0.18	0.32
$\frac{N_c}{c_*^2}$	0.08	0.26	0.21	0.11

Considering the TKE budget equation, Φ_u^T is in the same order of magnitude as the Φ^M and Φ_u^D for the Cases 1 and 4, showing the importance of this component in the variance budget for the convective and the stable ASL regimes. In Case 2, both Φ_u^T and Φ_u^D are one order of magnitude smaller than the values of Φ^M. For the tracers, $\Phi_{\chi_i}^T$ is one order of magnitude smaller than the magnitude of other budget components only for Case 1.

The dimensionless power spectra, based on 15-min segment chosen within the 30-min interval of Cases 1, 2, 3, and 4, are illustrated in Fig. 6, in which the estimated inertial subrange for each component is highlighted. It is observed that the subrange detector methodology satisfactorily identifies a range within the inertial subrange. Although the spectra present almost the same inertial subrange frequency interval for different tracers, this is not the case for the majority of segments used in this study. Therefore, the inertial subrange detector is implemented separately for each tracer.

The dimensionless spectra for the tracers collapsed on the examples for Cases 1, 2, and 3 (shown in Fig. 6a, b, and c, respectively). According to Table 3, the variation of Φ^T among these tracers are relatively small, as expected in the theory explained in Sect. 3.1, after the demonstration of Eq.
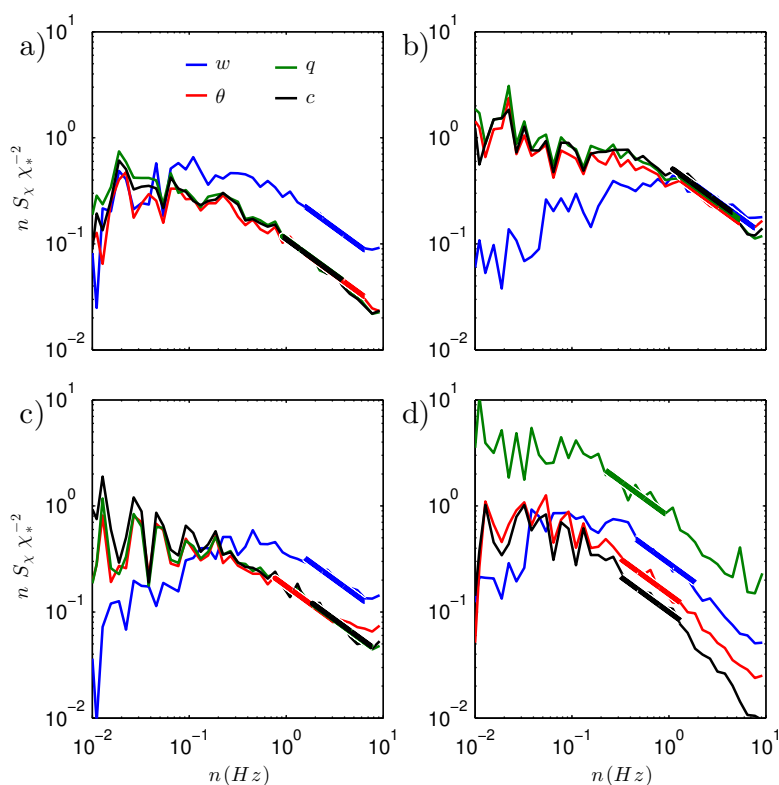
Figure 6. Dimensionless power spectra normalized by frequency (n [Hz]) and the respective characteristic scale squared (χ_*^{-2}) for vertical wind velocity (blue), virtual potential temperature (red), specific humidity (green), and specific CO_2 content (black). The thick lines indicate the non-linear $-2/3$ power slope fit within the inertial subrange. For each case we used 18,000 data points (15-min segment), collected at 20 Hz sampling rate during the BLLAST campaign at different days on June 2011: (a) 21st, 11 : 37 : 30 UTC; (b) 27th, 00 : 07 : 30 UTC; (c) 18th, 13 : 07 : 30 UTC; and (d) 18th, 22 : 37 : 30 UTC.

Atmospheric
Chemistry
and Physics
Discussions

(9). In Case 2 however, the transport component for the TKE is significantly different from the ones estimated for the tracers, although the spectra for w also collapsed (Fig. 6b). In this case, the ASL stability cannot be considered near-neutral (i.e. $\zeta \approx 0$), which is required in the theory for the cases

405 in that Φ^T is invariant also considering the TKE budget equation. Figure 6d, taken within the interval of Case 4 is an example where the spectra do not collapse. In this interval, Φ^T varies considerably among other tracers showing the same order of magnitude as the dynamical production of variance, Φ^H, in the budget equations.

5   Summary and outlook

410 This work brought an overview of how to estimate the dimensionless budget components of the variance equations for TKE, θ, q, and c using the EC and ID methods. Important features and peculiarities of each method were discussed in detail.

Among these features, we highlighted that if the transport and mechanical components are invariant to the tracer type, then the dimensionless power spectra normalized by the respective squared

415 characteristic scale collapse within the inertial subrange.

The results, based on the BLLAST dataset, suggested a set of parameterizations for the transport and dissipation rates of momentum and tracer variances. A linear relationship for the ASL stability range $-1 < \zeta < -0.1$ was proposed for the dimensionless dissipation component of all tracers in the form $\Phi^D_\chi \cong 0.4 + 0.2\zeta$. For the stable ASL regime, although it was observed an increased magnitude

420 of Φ^D and Φ^T, also for TKE, the results showed great discrepancies among the different tracers. Thus, we concluded that, in the stable and also near-neutral ASL stability regimes, $\Phi^T_{\chi_i}$ may not be considered identical for different tracers and Φ^T_u shall not be neglected.

Furthermore, the magnitudes of the characteristic scales of θ_*, q_*, and c_* are correlated to ζ, although the sign was not always the same. The friction velocity and the dissipation rate of TKE,

425 however, were observed to be more sensitive to the mean wind velocity than to the ASL stability regime. Therefore, we suggested that the parameterizations for Φ^D_u should include more mechanisms rather than only the ASL stability regime.

The described method for estimating each term of the turbulent fluxes and variances budget equations within the ASL has a wide range of applications. Two of them, however, deserve special atten-

430 tion: (i) for regions where the surface displacement length (d) is large, such as urban areas; and (ii) for data collected from moving platforms, such as buoys and ships.

Under the influence of canopy effects, the measurement height z has to be replaced by $z + d$, and therefore, it is crucial to appropriately determine d (Grimmond et al., 1998; Kanda et al., 2002; Gao and Bian, 2004). While several methodologies with their advantages and disadvantages have been

435 suggested, some iterative methods (Kanda et al., 2002) require a parameterization for Φ^D, such as the ones proposed in this study. Alternatively, d can be estimated iteratively by solving Eq. (5). In

Atmospheric
Chemistry
and Physics
Discussions

this scheme, Φ^M, Φ^T, Φ^D and ζ depend only on d, because the characteristic scales are estimated from Eqs. (12) and (13), the third-order moments in Φ^T are estimated from EC method, and the dissipation rate of TKE is calculated using the ID method.

440   For the sensors mounted on moving platforms, the contaminations induced by the platform motion have to be removed or at least to a large extent reduced before the calculation of fluxes, using motion correction algorithms (Edson et al., 1998; Huang et al., 2013; Miller et al., 2008; Prytherch et al., 2015). Although the inertial subrange may be considered isotropic and therefore invariant to platform motion, the elevation of the spectra at the motion-affected frequency band may induce anisotropy as a

445   noise. Thus, the whole spectrum is modulated and, as a consequence, the dissipation rates are usually overestimated (Bakhoday Paskyabi et al., 2013). This effect will be further enhanced for the offshore moored buoys where data might be collected within the wave boundary layer, and then additional corrections are required in order to account the wave-induced momentum flux (Bakhoday Paskyabi et al., 2015).

450   Appendix A: Inertial subrange detector method

It is crucial in the ID method to accurately resolve the inertial subrange. Therefore, we propose an iterative method to evaluate the variations of the independent constants α and β defined in Eqs. (14) and (15) by keeping constant values for the dissipation rates within a frequency interval, I. From the definition of the inertial subrange, both the dissipation rates and α, or β, are constant and therefore,

455   the boundaries of I can be defined evaluating the standard deviation of α, or β, in different regions of the spectra.

The spectra, calculated from 18,000 data sample collected at 20 Hz frequency rate, are divided into 48 frequency blocks (Table 4), which the number of estimates per block are logarithmically distributed, similar to the ones proposed by Kaimal and Gaynor (1983). For each block centered

460   frequency, n^*, the average power spectra, $\overline{S}(n^*)$, and the dissipation rate of TKE, $\epsilon^*(\overline{S_u}(n^*), n^*)$, are calculated using following equation, derived from the Kolmogorov power law.

$$\epsilon^* = \left(\frac{\overline{S_u}(n^*)}{\alpha} \right)^{\frac{3}{2}} n^{*\frac{5}{2}} \left(\frac{2\pi}{\overline{u}} \right). \tag{A1}$$

The iteration among the blocks consists of a loop starting in the centered frequency block $n^* = 0.0922$ Hz (index 22 in Table 4) and moving the interval I toward the higher frequencies, one block

465   per iteration, up to $n^* = 4.5244$ Hz (index 44). In this method, we suggest an interval I that includes nine consecutive blocks.

For each iteration, α is estimated for the nine n^* within I, keeping ϵ^* as a constant equal to the one corresponding to the fifth block from I (i.e. the block in the middle of I). Finally, the α standard deviation, σ_α, are calculated for each I.

Atmospheric
Chemistry
and Physics
Discussions

470   The inertial subrange is then defined as the I which has the smallest σ_α after finishing the iteration. If the smallest σ_α is greater than 10% of the true α, then we consider that the method cannot define an inertial subrange. The ϵ for the corresponding 30-min segment is then estimated according to the discussion in Sect. 3.3.

A similar procedure is done for estimating the I for the different tracers spectra. Since ϵ is now
475   known, the following Eq. (A2) is applied in an analogous way as it was described for Eq. (A1), but now estimating β, instead of α:

$$N_{\chi_i}^* = \left(\frac{\overline{S_{\chi_i}}(n^*)}{\beta} \right) \epsilon^{\frac{1}{3}} n^{*\frac{5}{3}} \left(\frac{2\pi}{\overline{u}} \right)^{\frac{2}{3}}. \tag{A2}$$

500

Table 4. Spectra logarithmic average smoothing for FFT result originated from 18,000 data sample collected at 20 Hz frequency rate.

Frequency block index	Number of estimates per block	Centered frequency n^* [Hz]
1	1	0.0011
2	1	0.0022
3	1	0.0033
4	1	0.0044
5	1	0.0056
6	1	0.0067
7	1	0.0078
8	1	0.0089
9	1	0.0100
10	1	0.0111
11	2	0.0128
12	3	0.0156
13	3	0.0189
14	3	0.0222
15	5	0.0267
16	5	0.0322
17	6	0.0383
18	7	0.0456
19	8	0.0539
20	11	0.0644
21	12	0.0772
22	15	0.0922
23	17	0.1100
24	21	0.1311
25	25	0.1567
26	29	0.1867
27	36	0.2228
28	42	0.2661
29	50	0.3172
30	61	0.3789
31	72	0.4528
32	86	0.5406
33	102	0.6450
34	122	0.7694
35	147	0.9189
36	174	1.0972
37	208	1.3094
38	249	1.5633
39	296	1.8661
40	355	2.2278
41	422	2.6594
42	505	3.1744
43	603	3.7900
44	719	4.5244
45	859	5.40111
46	1025	6.44778
47	1224	7.69722
48	1461	9.18889

Atmospheric
Chemistry
and Physics
Discussions

Open Access

References

Aubinet, M., Timo, V., and Dario, P.: Eddy covariance, Springer Netherlands, Dordrecht, doi:10.1007/978-94-007-2351-1, 2012.

Bakhoday Paskyabi, M., Flügge, M., Edson, J. B., and Reuder, J.: Wave–induced characteristics of atmospheric turbulence flux measurements, Energy Procedia, 35, 102–112, doi:10.1016/j.egypro.2013.07.163, 2013.

Bakhoday Paskyabi, M., Bryhni, H. T., Reuder, J., and Fer, I.: Lagrangian measurement of waves and near surface turbulence from acoustic instruments, Energy Procedia, 80, 141–150, doi:10.1016/j.egypro.2015.11.416, 2015.

Bloomfield, P.: Fourier analysis of time series, John Wiley & Sons, Inc., Raleigh, North Carolina, USA, 2 edn., 2000.

Bluteau, C. E., Jones, N. L., and Ivey, G. N.: Estimating turbulent kinetic energy dissipation using the inertial subrange method in environmental flows, Limnology and Oceanography: Methods, 9, 302–321, doi:10.4319/lom.2011.9.302, 2011.

Bumke, K., Schlundt, M., Kalisch, J., Macke, A., and Kleta, H.: Measured and parameterized energy fluxes estimated for Atlantic transects of R/V Polarstern, Journal of Physical Oceanography, 44, 482–491, doi:10.1175/JPO-D-13-0152.1, 2014.

Corrsin, S.: On the spectrum of isotropic temperature fluctuations in an isotropic turbulence, Journal of Applied Physics, 22, 469–473, doi:10.1063/1.1699986, 1951.

Dupuis, H., Taylor, P. K., Weill, A., and Katsaros, K.: Inertial dissipation method applied to derive turbulent fluxes over the ocean during the Surface of the Ocean, Fluxes and Interactions with the Atmosphere/Atlantic Stratocumulus Transition Experiment (SOFIA/ASTEX) and Structure des Echanges Mer-Atmosphere, Journal of Geophysical Research, 102, 21 115, doi:10.1029/97JC00446, 1997.

Dyer, A. J.: A review of flux-profile relationships, Boundary-Layer Meteorology, 7, 363–372, doi:10.1007/BF00240838, 1974.

Edson, J. B. and Fairall, C. W.: Similarity relationships in the Marine Atmospheric Surface Layer for terms in the TKE and scalar variance budgets*, Journal of the Atmospheric Sciences, 55, 2311–2328, doi:10.1175/1520-0469(1998)055<2311:SRITMA>2.0.CO;2, 1998.

Edson, J. B., Fairall, C. W., Mestayer, P. G., and Larsen, S. E.: A study of the inertial-dissipation method for computing air-sea fluxes, Journal of Geophysical Research, 96, 10 689, doi:10.1029/91JC00886, 1991.

Edson, J. B., Hinton, A. A., Prada, K. E., Hare, J. E., and Fairall, C. W.: Direct covariance flux estimates from mobile platforms at sea*, Journal of Atmospheric and Oceanic Technology, 15, 547–562, doi:10.1175/1520-0426(1998)015<0547:DCFEFM>2.0.CO;2, 1998.

Fairall, C. W. and Larsen, S. E.: Inertial-dissipation methods and turbulent fluxes at the air-ocean interface, Boundary-Layer Meteorology, 34, 287–301, doi:10.1007/BF00122383, 1986.

Foken, T.: 50 years of the Monin-Obukhov similarity theory, Boundary-Layer Meteorology, 119, 431–447, doi:10.1007/s10546-006-9048-6, 2006.

Foken, T., Göockede, M., Mauder, M., Mahrt, L., Amiro, B., and Munger, W.: Post-field data quality control, in: Handbook of Micrometeorology, 1988, pp. 181–208, Kluwer Academic Publishers, Dordrecht, doi:10.1007/1-4020-2265-4_9, 2005.

Atmospheric
Chemistry
and Physics
Discussions

540   Foken, T., Wimmer, F., Mauder, M., Thomas, C., and Liebethal, C.: Some aspects of the energy balance closure
        problem, Atmospheric Chemistry and Physics Discussions, 6, 3381–3402, doi:10.5194/acpd-6-3381-2006,
        2006.

        Gao, Z. and Bian, L.: Estimation of aerodynamic roughness length and displacement height of an urban surface
        from single-level sonic, Australian Meteorological Magazine, 53, 21–28, 2004.

545   Grimmond, C. S. B., King, T. S., Roth, M., and Oke, T. R.: Aerodynamic roughness of urban areas derived from
        wind observations, Boundary-Layer Meteorology, 89, 1–24, doi:10.1023/A:1001525622213, 1998.

        Hartogensis, O. K. and Bruin, H. A. R. D.: Monin–Obukhov similarity functions of the structure parameter
        of temperature and turbulent kinetic energy dissipation rate in the stable boundary layer, Boundary-Layer
        Meteorology, 116, 253–276, doi:10.1007/s10546-004-2817-1, 2005.

550   Hill, R. J.: Implications of Monin–Obukhov similarity theory for scalar quantities, Journal of the Atmospheric
        Sciences, 46, 2236–2244, doi:10.1175/1520-0469(1989)046<2236:IOMSTF>2.0.CO;2, 1989.

        Hill, R. J.: Algorithms for obtaining Atmospheric Surface-Layer fluxes from scintillation mea-
        surements, Journal of Atmospheric and Oceanic Technology, 14, 456–467, doi:10.1175/1520-
        0426(1997)014<0456:AFOASL>2.0.CO;2, 1997.

555   Högström, U.: Review of some basic characteristics of the atmospheric surface layer, Boundary-Layer Meteo-
        rology, 78, 215–246, doi:10.1007/BF00120937, 1996.

        Huang, Y., Song, J., and Fan, C.: A motion correction on direct estimations of air-sea fluxes froma buoy, Acta
        Oceanologica Sinica, 32, 63–70, 2013.

        Iwata, T., Yoshikawa, K., Higuchi, Y., Yamashita, T., Kato, S., and Ohtaki, E.: The spectral density tech-
560   nique for the determination of CO_2 flux over the ocean, Boundary-Layer Meteorology, 117, 511–523,
        doi:10.1007/s10546-005-2773-4, 2005.

        Kader, B. A.: Determination of turbulent momentum and heat fluxes by spectral methods, Boundary-Layer
        Meteorology, 61, 323–347, doi:10.1007/BF00119096, 1992.

        Kaimal, J. C. and Gaynor, J. E.: The Boulder Atmospheric Observatory, Journal of Climate and Applied Mete-
565   orology, 22, 863–880, doi:10.1175/1520-0450(1983)022<0863:TBAO>2.0.CO;2, 1983.

        Kaimal, J. C. J., Wyngaard, J. C. J., Izumi, Y., Coté, O. R., and Cote, O. R.: Spectral characteris-
        tics of Surface-Layer turbulence, Quarterly Journal of the Royal Meteorological Society, 98, 563–589,
        doi:10.1002/qj.49709841707, 1972.

        Kanda, M., Moriwaki, R., Roth, M., and Oke, T.: Area-averaged sensible heat flux and a new method to deter-
570   mine zero-plane displacement length over an urban surface using scintillometry, Boundary-Layer Meteorol-
        ogy, 105, 177–193, doi:10.1023/A:1019668424982, 2002.

        Kolmogorov, A. N.: Dissipation of energy in locally isotropic turbulencee, Dokl. Akad. Nauk SSSR, 32, 16–18,
        1941.

        Lee, X., Massman, W. J., and Law, B.: Handbook of micrometeorology, vol. 29 of *Atmospheric and Oceano-*
575   *graphic Sciences Library*, Springer Netherlands, Dordrecht, doi:10.1007/1-4020-2265-4, 2005.

        Li, M., Babel, W., Tanaka, K., and Foken, T.: Note on the application of planar-fit rotation for non-
        omnidirectional sonic anemometers, Atmospheric Measurement Techniques, 6, 221–229, doi:10.5194/amt-
        6-221-2013, 2013.

Lothon, M., Lohou, F., Pino, D., Couvreux, F., Pardyjak, E. R., Reuder, J., Vilà-Guerau de Arellano, J., Durand,
580   P., Hartogensis, O., Legain, D., Augustin, P., Gioli, B., Faloona, I., Yagüe, C., Alexander, D. C., Angevine,
W. M., Bargain, E., Barrié, J., Bazile, E., Bezombes, Y., Blay-Carreras, E., van de Boer, A., Boichard, J. L.,
Bourdon, A., Butet, A., Campistron, B., de Coster, O., Cuxart, J., Dabas, A., Darbieu, C., Deboudt, K.,
Delbarre, H., Derrien, S., Flament, P., Fourmentin, M., Garai, A., Gibert, F., Graf, A., Groebner, J., Guichard,
F., Jimenez Cortes, M. a., Jonassen, M., van den Kroonenberg, A., Lenschow, D. H., Magliulo, V., Martin,
585   S., Martinez, D., Mastrorillo, L., Moene, a. F., Molinos, F., Moulin, E., Pietersen, H. P., Piguet, B., Pique, E.,
Román-Cascón, C., Rufin-Soler, C., Saïd, F., Sastre-Marugán, M., Seity, Y., Steeneveld, G. J., Toscano, P.,
Traullé, O., Tzanos, D., Wacker, S., Wildmann, N., and Zaldei, A.: The BLLAST field experiment: Boundary-
Layer Late Afternoon and Sunset Turbulence, Atmospheric Chemistry and Physics Discussions, 14, 10 789–
10 852, doi:10.5194/acpd-14-10789-2014, 2014.
590   Miller, S. D., Hristov, T. S., Edson, J. B., and Friehe, C. A.: Platform motion effects on measurements of
turbulence and air–sea exchange over the open ocean, Journal of Atmospheric and Oceanic Technology, 25,
1683–1694, doi:10.1175/2008JTECHO547.1, 2008.
Nilsson, E., Lothon, M., Lohou, F., Pardyjak, E., Hartogensis, O., and Darbieu, C.: Turbulence kinetic energy
budget during the afternoon transition &ndash; Part 2: A simple TKE model, Atmospheric Chemistry
595   and Physics Discussions, 15, 29 807–29 869, doi:10.5194/acpd-15-29807-2015, 2015.
Norman, M., Rutgersson, A., Sørensen, L. L., and Sahlée, E.: Methods for estimating air–sea fluxes of CO_2 us-
ing high-frequency measurements, Boundary-Layer Meteorology, 144, 379–400, doi:10.1007/s10546-012-
9730-9, 2012.
Ohtaki, E.: On the similarity in atmospheric fluctuations of carbon dioxide, water vapor and temperature over
600   vegetated fields, Boundary-Layer Meteorology, 32, 25–37, doi:10.1007/BF00120712, 1985.
Pahlow, M., Parlange, M. B., and Porté-Agel, F.: On Monin–Obukhov similarity in the stable Atmospheric
Boundary Layer, Boundary-Layer Meteorology, 99, 225–248, doi:10.1023/A:1018909000098, 2001.
Prytherch, J., Yelland, M. J., Brooks, I. M., Tupman, D. J., Pascal, R. W., Moat, B. I., and Norris, S. J.: Motion-
correlated flow distortion and wave-induced biases in air–sea flux measurements from ships, Atmospheric
605   Chemistry and Physics, 15, 10 619–10 629, doi:10.5194/acp-15-10619-2015, 2015.
Ruppert, J., Thomas, C., and Foken, T.: Scalar similarity for relaxed eddy accumulation methods, Boundary-
Layer Meteorology, 120, 39–63, doi:10.1007/s10546-005-9043-3, 2006.
Sahlée, E., Smedman, A.-S., Rutgersson, A., and Högström, U.: Spectra of CO_2 and water vapour in the Marine
Atmospheric Surface Layer, Boundary-Layer Meteorology, 126, 279–295, doi:10.1007/s10546-007-9230-5,
610   2008.
Sorbjan, Z.: Improving non-local parameterization of the convective boundary layer, Boundary-Layer Meteo-
rology, 130, 57–69, doi:10.1007/s10546-008-9331-9, 2009.
Sørensen, L. L. and Larsen, S. E.: Atmosphere–surface fluxes of CO_2 using spectral techniques, Boundary-
Layer Meteorology, 136, 59–81, doi:10.1007/s10546-010-9499-7, 2010.
615   Sørensen, L. L., Jensen, B., Glud, R. N., McGinnis, D. F., Sejr, M. K., Sievers, J., Søgaard, D. H., Tison, J.-L.,
and Rysgaard, S.: Parameterization of atmosphere–surface exchange of CO_2 over sea ice, The Cryosphere,
8, 853–866, doi:10.5194/tc-8-853-2014, 2014.

Atmospheric
Chemistry
and Physics
Discussions

Open Access

EGU

Stull, R. B.: An introduction to boundary layer meteorology, vol. 13, Springer Netherlands, Dordrecht, doi:10.1007/978-94-009-3027-8, 1988.

620 Willis, G. E. and Deardorff, J. W.: On the use of Taylor's translation hypothesis for diffusion in the mixed layer, Quarterly Journal of the Royal Meteorological Society, 102, 817–822, doi:10.1002/qj.49710243411, 1976.

Wyngaard, J. C. and Coté, O. R.: The budgets of turbulent kinetic energy and temperature variance in the Atmospheric Surface Layer, Journal of the Atmospheric Sciences, 28, 190–201, doi:10.1175/1520-0469(1971)028<0190:TBOTKE>2.0.CO;2, 1971.

625 Yelland, M. and Taylor, P. K.: Wind stress measurements from the open ocean, Journal of Physical Oceanography, 26, 541–558, doi:10.1175/1520-0485(1996)026<0541:WSMFTO>2.0.CO;2, 1996.

Zilitinkevich, S. and Calanca, P.: An extended similarity theory for the stably stratified atmospheric surface layer, Quarterly Journal of the Royal Meteorological Society, 126, 1913–1923, doi:10.1002/qj.49712656617, 2000.